LAWRENCE
LIVERMORE
NATIONAL
LABORATORY

LLNL-JRNL-674038

Precision Photothermal Annealing of Nanoporous Gold Thin Films for the Microfabrication of a Single-chip Material Libraries

C. D. Harris, N. Shen, A. Rubenchik, S. G. Demos, M. J. Matthews

June 30, 2015

Nanoscale

Disclaimer

Precision Photothermal Annealing of Nanoporous Gold Thin Films for the Microfabrication of Single-chip Material Libraries

Single-chip material libraries of thin films of nanostructured materials are a promising approach for high throughput studies of structure-property relationship in the fields of physics and biology. Nanoporous gold (np-Au), produced by an alloy corrosion process, is a nanostructured material of specific interest in both these fields. One attractive property of np-Au is its self-similar coarsening behavior by thermally induced surface diffusion. However, traditional heat application techniques for the modification of np-Au are bulk processes that cannot be used to generate a library of different pore sizes on a single chip. Here, laser micromachining offers an attractive solution to this problem by providing a means to apply energy with high spatial and temporal resolution. In the present study we use finite element multiphysics simulations to predict the effects of laser mode (continuous-wave vs. pulsed) and supporting substrate thermal conductivity on the local np-Au film temperatures during photothermal annealing and subsequently investigate the mechanisms by which the np-Au network is coarsening. The simulations predict that continuous-wave mode laser irradiation on a silicon supporting substrate supports the widest range of morphologies that can be created through the photothermal annealing of thin film np-Au. Using this result we successfully fabricate a single-chip material library consisting of 81 np-Au samples of 9 different morphologies for use in increased throughput material interaction studies.

Keywords

During the past decade, nanoscale materials have attracted significant interest for their unique structure-mediated properties. Porous metals have become of particular interest for applications in energy and biology research. One of these materials is nanoporous gold (np-Au), a material that has attracted much interest for its applications in electrochemical sensors,[1-5] catalysis,[1, 6] tunable molecular release,[7-8] structure property studies at the nanoscale,[5, 9-10] as well as biomaterial interfaces.[11-13] Np-Au is produced through an alloy corrosion process known as dealloying,[14] that generates a characteristic three dimensional nanoscale network of pores and ligaments. Microscopically, the porosity of np-Au is caused by a rearrangement of gold atoms during the dealloying process where gold atoms actively diffuse towards a lower energy state.[14-15] The pore and ligament size distributions can be controlled through both altering dealloying parameters (i.e. temperature, time, and acid concentration) as well as post-fabrication annealing through the application of energy.[16-19] Previous studies have demonstrated these morphology modification processes in both bulk (micrometer-scale thickness) and thin film (nanometer-scale thickness) np-Au.[1, 20-21] Here we investigate a method for creating of a single-chip np-Au material library which requires local control of heat to achieve controllable morphology modification on a single chip. Laser micro-machining provides the required spatial and temporal control of depositing energy near the surface of the material, and thus already has gained significant traction as a highly controllable and precise method to cut, anneal, and modify materials.[22-25] Inspired by recent work on laser-induced modification of ligament and pore size distributions of bulk np-Au,[20] the present study focuses on effects that arise when working with thin supported np-Au coatings. Ultimately, this work aims to characterize the effect of controlled photothermal annealing on thin film np-Au coatings in order to fabricate single-chip material

libraries of morphologically modified thin film np-Au coatings for future use in high throughput investigation of structure-property relationships.

Results and Discussion

Laser-based photothermal annealing is accomplished through the local exposure and absorption of laser energy. This localized surface heating is caused primarily due to the absorption of photons by the material. Laser heating during annealing on non-structured surfaces has been extensively studied and generalized equations of the laser heating profile on many different materials have been presented. However, modeling laser heating on heat sensitive nanostructured surfaces, such as np-Au, during the annealing process presents many challenging scenarios that must be considered.

Laser coupling to np-Au surface

At the foundation of the photothermal heating of a material is the effectiveness of laser coupling to the material surface. The amount of energy that can be transferred to the material surface is determined by the efficiency of laser coupling to the material surface, commonly known as the absorbance. Typically, absorbance ($A_b = 1 - R_b$) of the bulk material, with R_b being material reflectivity, is used to linearly scale the power that is coupled to the material surface. The reflectivity of standard np-Au at a wavelength of $\lambda = 532$ nm has been calculated in previous studies as $R_{np\text{-}Au} = 0.22$. However, as np-Au anneals due to the heating, the reflectivity approaches the value of planar Au given by $R_{pl\text{-}Au} = 0.62$. This increase in reflectivity during laser exposure can potentially account for up to a 40% decrease in laser energy being transferred into the np-Au film during photothermal treatment. However, to our knowledge no comprehensive models capable of predicting the changes in np-Au reflectivity during thermal coarsening have been created. Since the film morphologies of np-Au that were obtained in this paper are still in a notably porous regime, the general reflectivity of the beginning np-Au film have been used to calculate absorbance in the following models. Additionally, since a shift in the reflectivity towards that of planar Au would cause less heating of the film we consider that the modeled coupling in this case would be the scenario of maximal energy transfer through the entire application of energy.

Heat transfer in the np-Au film

To model the heat transfer in the np-Au film due to laser induced surface heating the thermal conductivity of np-Au, $\kappa_{np\text{-}Au}$, must be determined. The thermal conductivity of np-Au and the effect of thermal treatment on the thermal conductivity has been extensively studied previously.[26-27] Here, we use the calculations performed by Hopkins et al. to calculate the thermal conductivity of the np-Au film.[27] Briefly, this method uses the product of two scaling ratios to determine the conductivity of np-Au at a given ligament diameter. The ligament diameter of the np-Au films used in this study is on the order of 50 nm as reported previously by our group.[11, 21] First, the ratio of the reduced conductivity due to ligament diameter, κ_w, to the bulk conductivity, κ_b, is calculated by

$$\frac{\kappa_w}{\kappa_b} \approx 1 - \frac{3}{4u} + \frac{3}{8u^3}$$

where u is the ratio of the ligament diameter, d, to the electron mean free path in the ligament, λ. It is worth noting that this equation holds only for values of $u > 1$. Using bulk conductivity, κ_b, of Au (317 W m^{-1} K^{-1}) the reduced conductivity κ_w is found to be 190.2 W m^{-1} K^{-1}. Next the ratio of decrease due to porous volume is calculated using the equation

$$\frac{\kappa_p}{\kappa_w} = (1 - f)^{3/2}$$

where f is the porosity and κ_p is the final thermal conductivity of np-Au ($\kappa_{np\text{-}Au}$). Using a porosity of 50% for the films used in this study, obtained through image analysis approximation, a value of 67.14 W m^{-1} K^{-1} is determined for np-Au thermal conductivity. Subsequent analysis for larger 200 nm diameter ligament np-Au (thermally coarsened) reveals an increase in np-Au thermal conductivity to 95.12 W m^{-1} K^{-1}, a 41.6% increase in conductivity. This means that similarly to reflectivity the thermal conductivity also increases during annealing. However, because this system consists of a thin 600 nm np-Au film and a thick 500 μm supporting material heat transport in the system is dominated by the conduction of heat into the supporting material and not laterally through the np-Au film.

Another important factor to consider in the heat transfer to the np-Au film is the mode of the laser being used to irradiate the sample surface. Energy can be applied through either a continuous-wave (CW) or pulsed mode laser beam. Typically, CW irradiation is used in applications where extended heating and steady application of energy is needed whereas pulsed lasers are used in cutting applications due to the fast pulse time (nanosecond to femtosecond) limiting the extent of excess thermal damage caused by the energy application. In order to investigate both the temporal and spatial film temperature distribution as a function of laser mode COMSOL, a finite element multiphysics modeling program, was used to create a mode simulating the application of both laser modes using parameters seen in the supporting information.

Finally, the laser beam must be modeled as a Gaussian heating profile to accurately obtain the heating profile in the film. In order to accurately model the Gaussian profile of the beam the power was scaled as a function of the ratio of radial beam intensity to maximum intensity given by,

$$\frac{I}{I_{max}} = \exp\left(-\frac{8r^2}{d^2}\right)$$

where r corresponds to the radial position relative to the center of the Gaussian laser beam and d to the laser spot diameter.

Simulations were performed at P_{cw} = 1 W, 750 mW, and 500 mW for the CW mode as well as E_p = 0.25 J/cm^2 and 0.025 J/cm^2 for pulsed mode. These powers correspond to 80%, 60%, and 40% of maximum operating power for CW whereas the pulse energies used correspond to 1% and 0.1% power for the pulsed mode. Film temperatures from this model were taken at 6 points (0, 0.5, 1, 1.5, 2, and 2.5 μm) along the Gaussian profile of the surface heating. These film

temperatures represent the maximum temperatures that are experienced in the np-Au film temporally over the radial distribution of the laser beam.

A comparison between CW and pulsed mode laser irradiation on silicon reveals distinctly different heat transport through the np-Au film (Figure 1 A & C) and temperature profiles (Figure 1 D,G,J & F,I,L). The main reason for this difference is the duration of energy application, 10 ms for CW exposure vs. 9 ns for pulsed exposure. The long exposure of CW irradiation leads to a steady state temperature profile for the majority of the duration of energy application. Conversely, the extremely short duration of the pulsed irradiation leads to a spike in film temperature with the film never reaching a steady state value before the exposure is over. Another key difference between irradiation in CW and pulsed modes (at least for the systems used in this study) is the large difference between energy densities of the laser systems. At 1 W (80% system power) the CW laser irradiation maintains steady state film temperatures across the entire radial beam distance that are under the melting point of Au (T_m = 1337 K), whereas at 0.25 J/cm^2 (1% system power) pulsed laser irradiation increases the film temperature to more than four times the melting temperature of Au. Decreasing the pulsed laser energy density to 0.025 J/cm^2 (0.1% system power) is required to maintain film temperatures in a regime similar to that of 1 W CW mode irradiation. This result is not surprising seeing as pulsed mode lasers are typically used for cutting applications due to the fast application of high energy density damaging irradiation while maintaining low thermal damage due a long duration between pulses.

Another important variable that must be considered is the thermal conductivity of the supporting substrate. Previously, studies on photohermal annealing of np-Au used thick (200 μm) unsupported disks and therefore did not need to account for temperature differences in the film due to underlying substrate. The two most commonly used supporting substrates for thin film np-Au are generally silicon and glass. Using glass as the supporting substrate decreases the thermal conductivity from 149 W m^{-1} K^{-1} to 1.47 W m^{-1} K^{-1} an approximately hundred-fold decrease in conductivity. These simulations demonstrate that changing the supporting substrate from a thermally conductive material (silicon) to a less thermally conductive material (glass) causes large differences in heat transport and thus local temperature. In glass-supported films, heat does not get transported into the bulk supporting material as readily, which causes the build-up of heat in the area under and surrounding the laser spot (Figure 1 B). This build-up of heat in the np-Au film increases the film temperatures far beyond that of what is seen in np-Au supported on silicon. Even with a 2.5-fold reduction in laser power at 400 mW the glass substrate causes the np-Au film to reach temperatures above the melting point of Au. However, lower powers of 200 and 100 mW reach a steady state value below the melting temperature of Au. This suggests that in changing the thermal conductivity of the supporting substrate the range of powers needed to control the annealing of np-Au is shifted to a lower and narrower range of powers. Additionally, unlike np-Au supported by a silicon substrate, the np-Au film on glass takes a longer time to reach a steady state temperature (Figure 1 E, H, K) which is characteristic of the heat building up in the np-Au film due to lack of a highly conductive sink material. Here, we have simulated the heat transfer in thin film np-Au under multiple model conditions of changing laser mode and substrate thermal conductivity. This enables the investigation of the dominant np-Au film coarsening mechanisms during photothermal annealing.

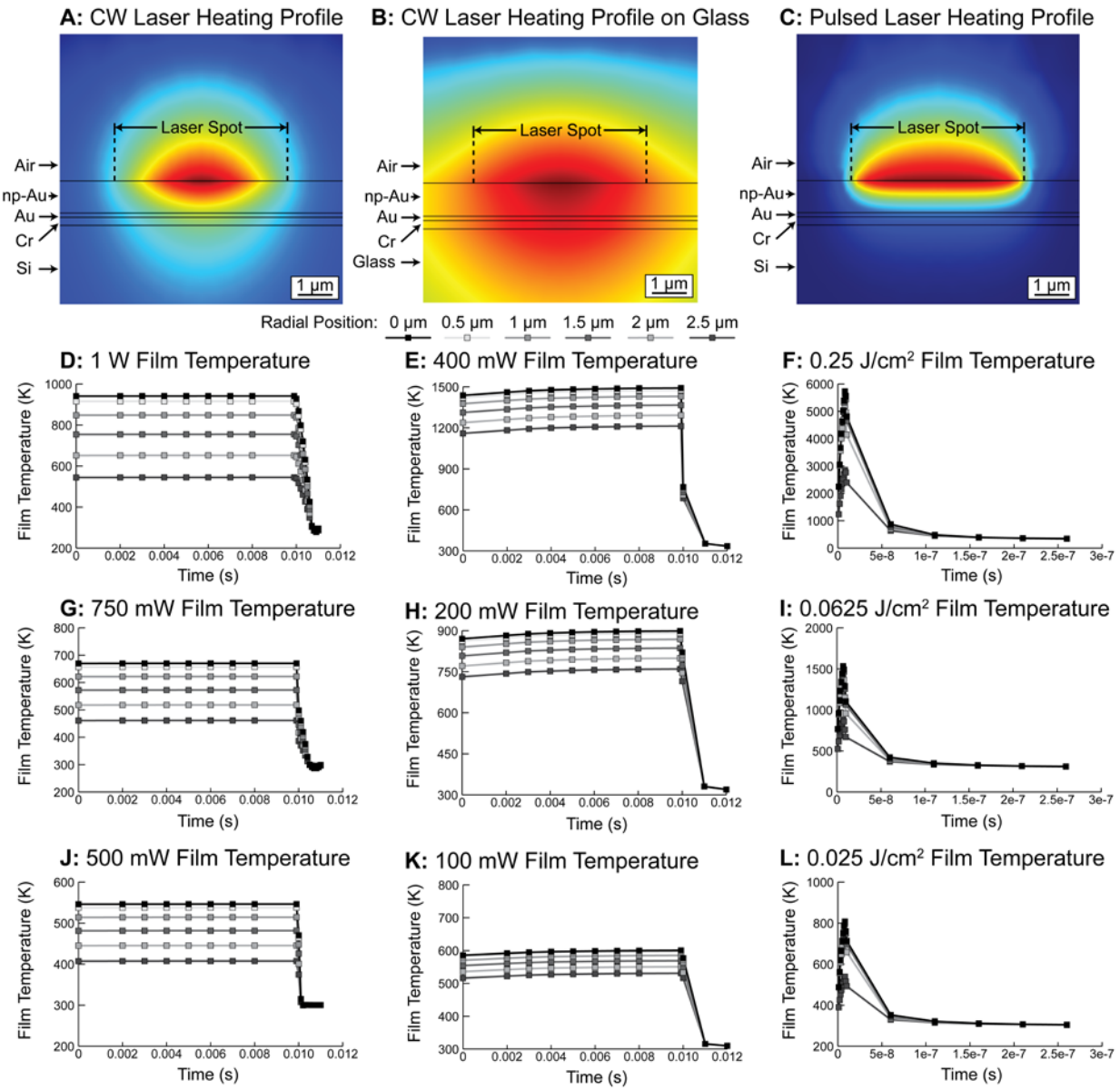

Figure 1. Simulated heat distribution in np-Au film in response to CW laser irradiation on both silicon (A) and glass (B) as well as pulsed mode laser irradiation on silicon (C). Resulting film temperature profiles are shown for 1 W (C), 750 mW (G), 500 mW (J), and 400 mW (E), 200 mW (H), 100 mW (K) in the CW mode on silicon and glass respectively, and 0.25 J/cm^2 (F), 0.0625 J/cm^2 (I), 0.025 J/cm^2 (L) in the pulsed mode on silicon.

Mechanisms of mass transport in np-Au film during photothermal annealing

The coarsening of np-Au can primarily happen through two mechanisms: curvature driven surface diffusion for temperatures below the melting temperature and surface tension driven viscous flow for temperatures above the melting point (Figure 2). For our purpose of creating controllable np-Au morphologies, coarsening through surface diffusion is the desired mechanism because it provides superior feature size control through controlling the diffusion kinetics. Melting, by contrast, is a first order phase transition causing abrupt mass transport property changes.

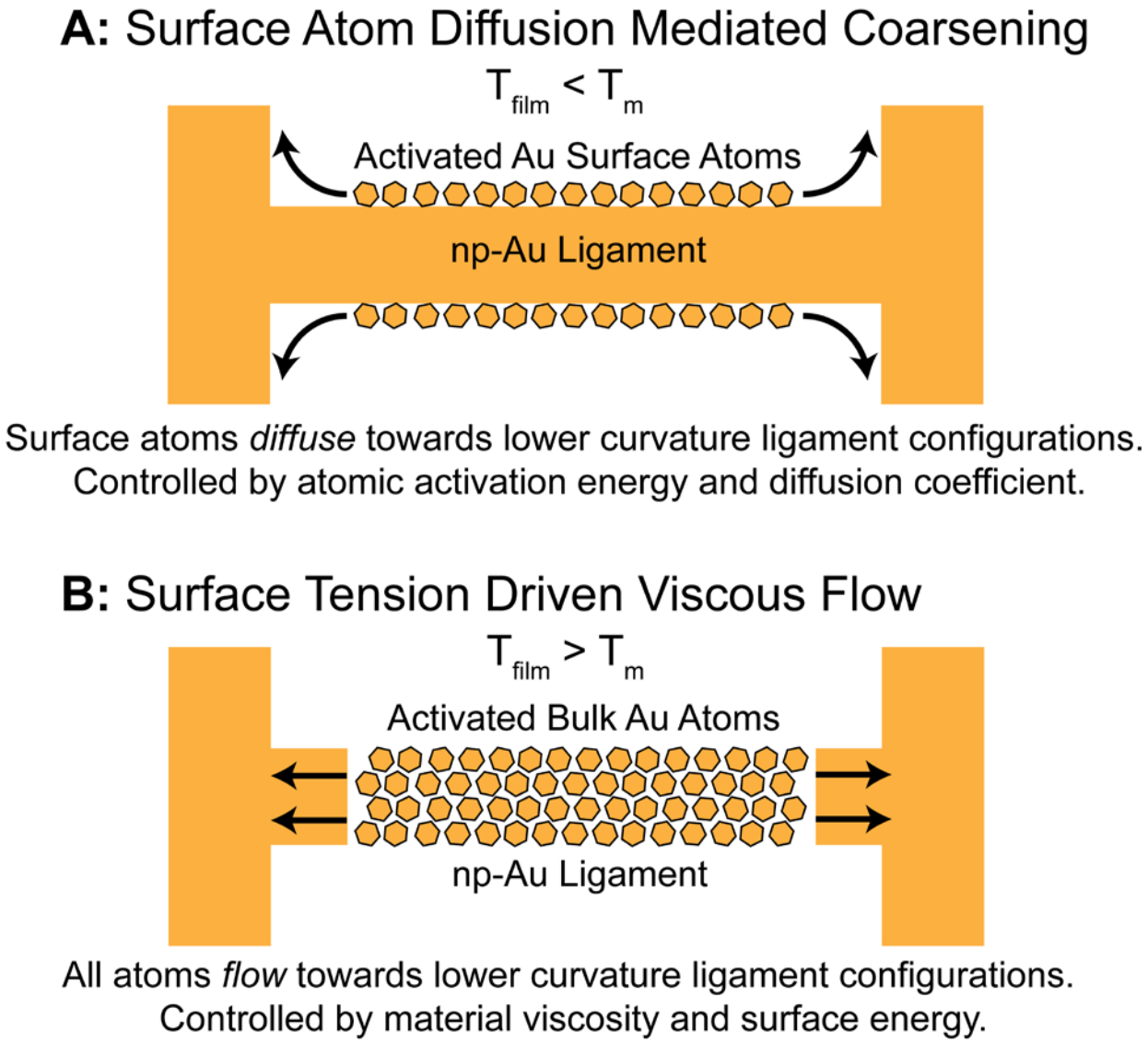

Figure 2. Diagram illustrating surface atom diffusion mediated coarsening (A) and surface tension driven viscous flow (B).

Because surface diffusion is a relatively slow process, appreciable coarsening of the material in the surface diffusion regime, requires that the local temperatures are raised to values close to the melting point for at least multiple milliseconds Therefore, it is essential to identify process parameters that achieve stable local temperature profiles on the millisecond time scale.

The simulations reveal that both CW and pulsed mode laser heating for the conditions discussed above result in film temperatures below the melting point with the exception of 400 mW CW mode on glass and the 0.25 J/cm^2 pulsed mode exposure. However, the exposure time depends drastically on the laser mode with CW heating resulting in six orders of magnitude longer exposures than pulsed mode exposure. To further investigate the surface atom diffusion occurring in the diffusion coefficients of the film over time can be calculated. The diffusion

coefficient of Au has been characterized previously[28] to follow an Arrhenius relationship with the temperature of the material given by

$$D = D_o \exp\left(-\frac{E_A}{k_b T}\right)$$

where D_o is a pre-exponential factor empirically determined to be 5 x 10^{-12} m^2 s^{-1}, E_A is the activation energy of gold 0.4 eV or 6.41 x 10^{-20} J, k_b is the Boltzmann constant 1.38 x 10^{-23} J K^{-1}, and T is the temperature of the material. Using this equation, the diffusion coefficient can be determined as a function of changing film temperature over time (Figure 3).

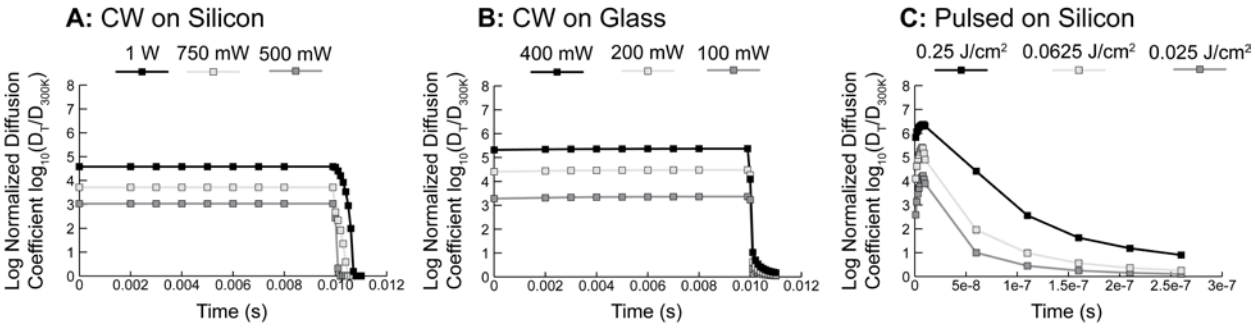

Figure 3. Normalized diffusion coefficient over the time course of photothermal annealing at r = 0 μm for each simulated laser mode demonstrates distinct differences between the temporal activation of the np-Au film.

Clearly, only CW exposure results in sufficiently high (and stable) diffusion coefficients over sufficiently long times. On the other hand, although the pulsed laser does reach temperatures that enable rapid surface diffusion the associated time-scale is much too short to allow for appreciable coarsening. Going further, the square root of the integral of the diffusion coefficient function can be taken to determine a characteristic diffusion length associated with the simulated results.

Table 1. Characteristic diffusion length values for each simulated laser mode and substrate

CW on silicon	Diffusion Length
1 W	59.18 nm
750 mW	20.01 nm
500 mW	9.12 nm
CW on glass	
400 mW	130.64 nm
200 mW	47. 58 nm
100 mW	13.24 nm
Pulsed on silicon	
0.25 J/cm^2	0.42 nm
0.0625 J/cm^2	0.11 nm
0.025 J/cm^2	0.026 nm

Although there is no direct relationship between the surface diffusion coefficient and resulting pore morphology, these calculations (shown in Table 1) demonstrate the difference between CW and pulsed mode laser irradiation for the efficacy of surface diffusion mediated thermal coarsening in np-Au films. The sub-nanometer values seen for the pulsed laser suggest that any annealing that happens during photothermal annealing would in fact be viscous flow-dominated and not surface atom diffusion-dominated. Therefore it is very unlikely that pulsed mode laser irradiation can result in subtle morphological changes, but rather results in the flow of the film towards bulk Au in a very short time period, an interesting result but not highly useful for engineering morphology libraries.

Morphology and analysis of photothermally annealed np-Au films

Using the parameters used in the simulations, np-Au thin films were fabricated on both silicon and glass supporting substrates. These samples were then annealed using either CW or pulsed mode laser irradiation using a custom set-up for CW mode (Figure S1) and a New Wave Research (Fremont, CA) laser mill for pulsed mode irradiation. The resulting morphology changes, visualized through SEM, are distinctly different for different annealing parameters, most notably between CW and pulsed mode annealing. Additionally, large changes to the coarsening distributions, analyzed through a custom MATLAB script that calculated ligament width as an average over the track length, are seen in pulsed mode compared to CW (Figure 4).

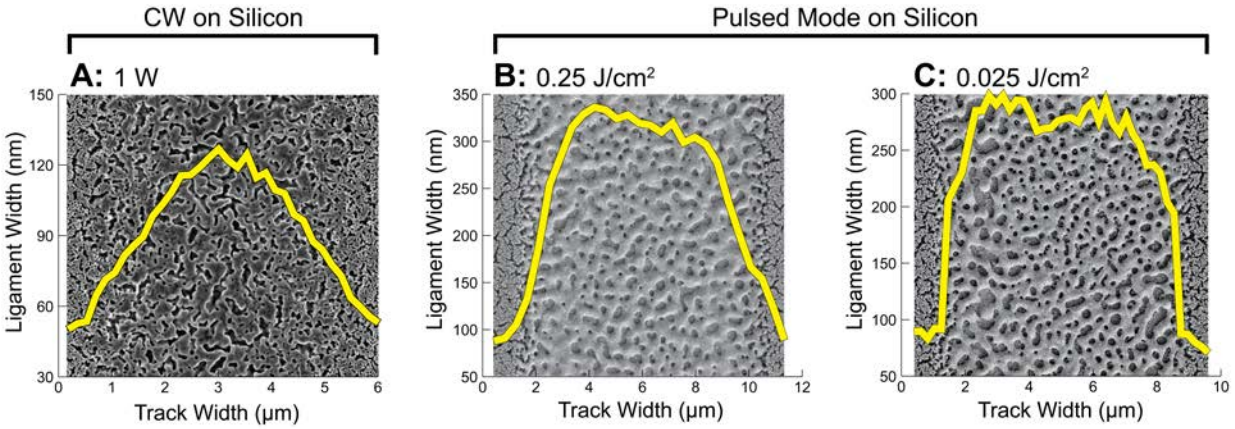

Figure 4. Scanning electron micrographs of thin film np-Au on silicon photothermally annealed by CW (A) and pulsed (B & C) mode laser irradiation. Images illustrate the noticeable differences in ligament size over the width of the annealing tracks between the two modes.

As expected from the previous analysis, 0.25 J/cm^2 pulsed mode irradiation (Figure 4 B) leads to local melting of the np-Au film rather than controllable coarsening as seen for 1 W CW irradiation (Figure 4 A). Interestingly, the lower pulsed energy density used in the simulations (0.025 J/cm^2) also led to complete sintering of the np-Au film contrary to the simulated film temperatures staying well below the melting temperature of Au. This is most easily explained by the power limitations of the pulsed laser system used for this study: at 0.025 J/cm^2 the system is running at 0.01% full power thus most likely leading to unstable operating conditions. Given the diffusion length analysis (Table 1) it is however highly unlikely the short pulse duration can produce any meaningful coarsening of the np-Au film. To achieve appreciable coarsening of np-

Au with a pulsed mode laser would require a high repetition rate along with an extremely low power density, which essentially converges the pulsed mode to a CW laser.

Many models exist to capture both the viscous and diffusion related rearrangement of nanostructured surfaces in an analytical model. Therefore, it is possible to qualitatively validate that this difference in morphology is stemming from pulsed irradiation leading to viscous flow of np-Au whereas surface atom diffusion is the dominating mechanism in CW irradiation. Cassidy et al.[29] posit a simple model for the general smoothing kinetics of uniformly repeating structures on glass. Briefly, the time course function of the changing surface structure is a function of the Fourier space power spectrum given by

$$C_n(t) = C_n(0)\exp -[B(n\omega)^4 + F(n\omega)]t$$

where C_n(t) and C_n(0) are the power spectral density functions from the 2D Fourier transform of the ending and beginning surface morphologies respectively, B is the scaling factor for surface atom diffusion smoothing and F is the scaling factor for capillary (viscous) flow smoothing.

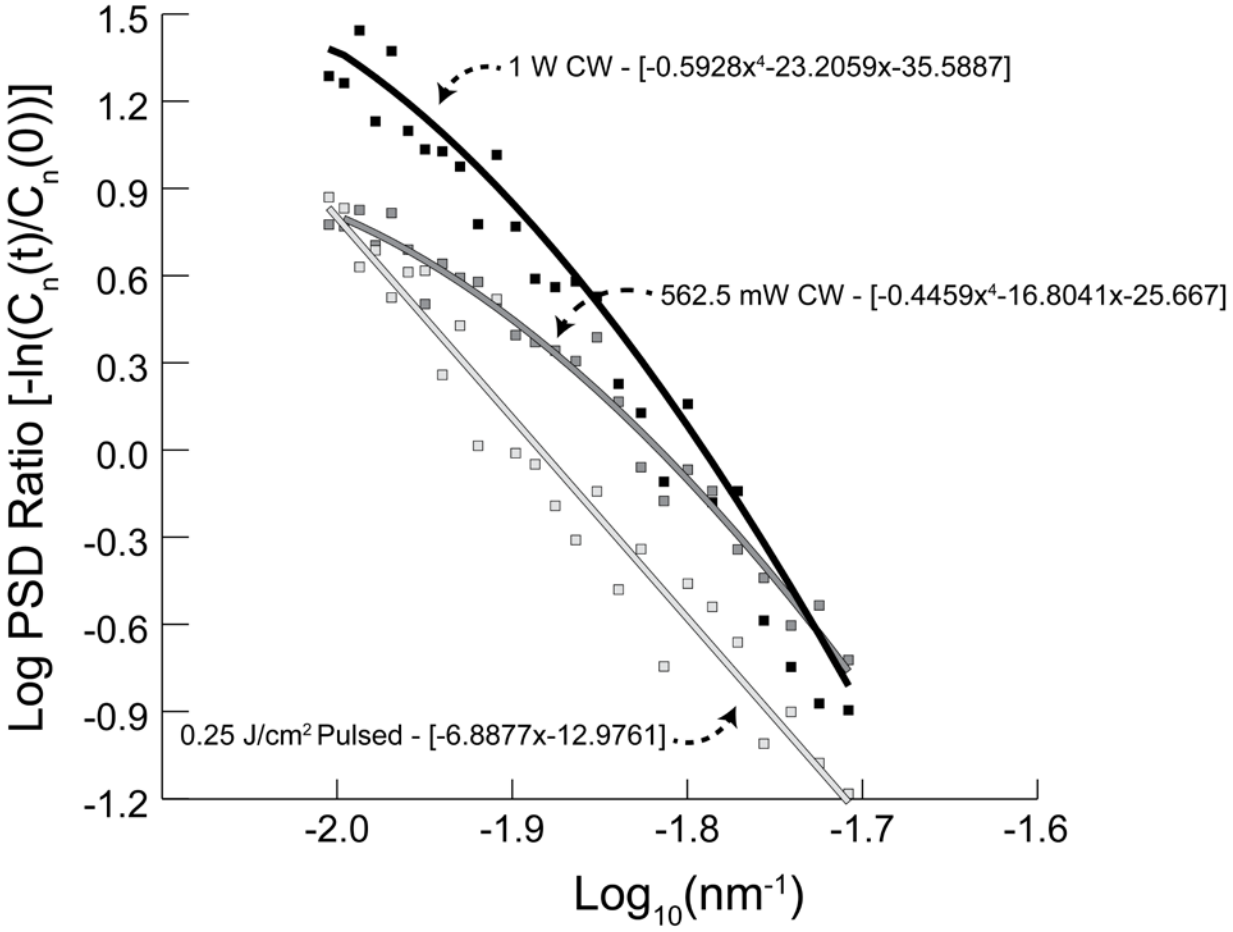

Figure 5. Plotted log ratio of PDS function further suggests differences in the smoothing dynamics between CW and pulsed mode annealing. Fit equations are given in square brackets and show clear differences in smoothing mechanisms between the two laser modes.

Plotting the natural log of the PSD ratio between samples annealed with CW and pulsed irradiation and their original starting morphologies reveals that pulsed mode behaves in a mostly linear regime for the entirety of the spatial frequencies tested, whereas CW annealing introduces a quartic relationship (surface diffusion) to the smoothing model (Figure 5). This suggests again that pulsed mode irradiation is coarsening only through bulk viscous flow of the Au in the film and not through surface atom diffusion.

Investigating the effect of substrate thermal conductivity yields results consistent with the simulations, with the power range that leads to controlled morphology changes being much smaller for glass (130 mW to 47 mW) than for silicon substrates (500 mW to 1 W). Interestingly, the range of powers determined experimentally for the glass substrate was about 25% lower than the simulated power where the np-Au film temperatures were indicative of np-Au coarsening (Figure 6).

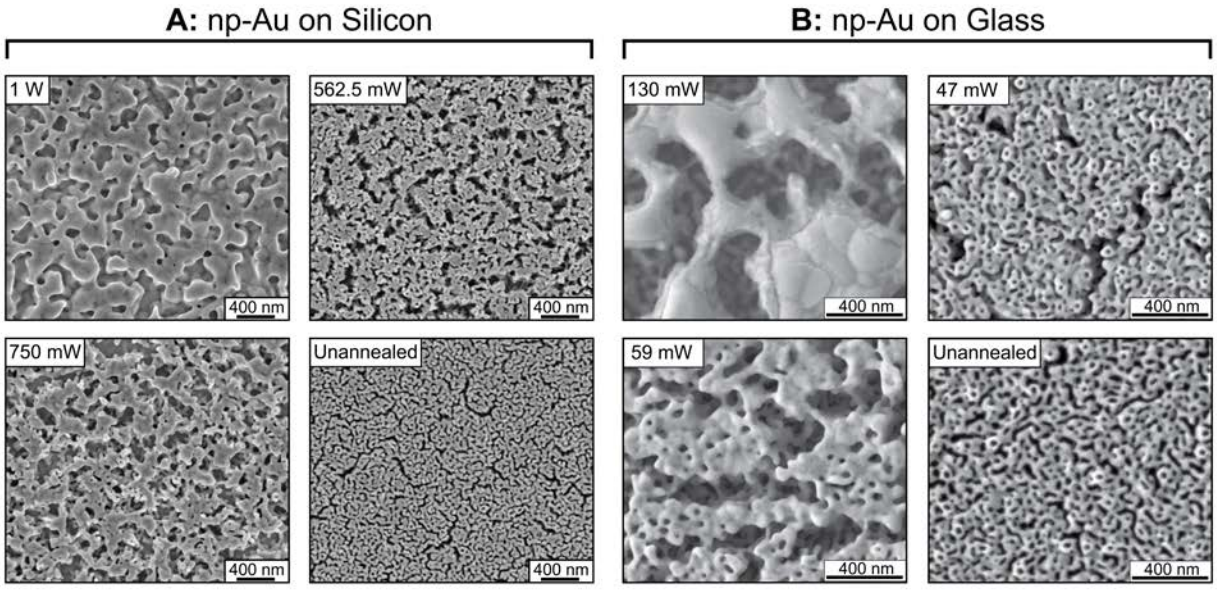

Figure 6. Np-Au thin film coatings supported on both silicon (A) and glass (B) demonstrate drastically different ranges of powers needed for control over np-Au morphology through photothermal annealing.

This can potentially be explained by differences in the glass used experimentally and in the simulation model resulting in an even lower thermal conductivity of the glass during these experiments. Regardless, this result clearly demonstrates that silicon as a substrate enables the widest range of powers to be used to create multiple morphologies of np-Au. Now that the supporting substrate and laser mode have been selected np-Au material libraries of morphologies on a single chip can be fabricated using precise photothermal annealing.

Material library fabrication

Guided by our simulations and preliminary experimental data, we fabricated a single chip material library of np-Au thin film coating morphologies. A 9 by 9 array of 81 different np-Au

squares ranging from 1 mm^2 to 0.04 mm^2 was fabricated onto a single 20 mm square silicon chip (Figure 7 A). Each chip was then annealed using a fully automated LabVIEW script with decreasing laser power per row. Starting at P_{cw} = 1 W and decreasing to P_{cw} = 562.5 mW by the final row, with a constant stage velocity of 500 μm/s and beam diameter of 5 μm. The entire surface was annealed through rastering of the laser back and forth across the np-Au surface with raster spacing starting at 5 μm (P_{cw} = 1 W) and ending at 2.5 μm (P_{cw} = 562.5 mW). This decrease in raster spacing is necessary to account for the decreasing power input from the laser, and therefore the decreasing of the effective laser spot size, to ensure uniform annealing across the entire np-Au surface. Annealing of the entire chip was done in a single 14 hour run. The long processing time is primarily due to the small spot size of the laser used in this study and could be dramatically decreased by using a larger spot size (or smaller samples). After annealing, each square on the material library was imaged and characterized for changes in both ligament width and pore diameter (Figure 7 C & D).

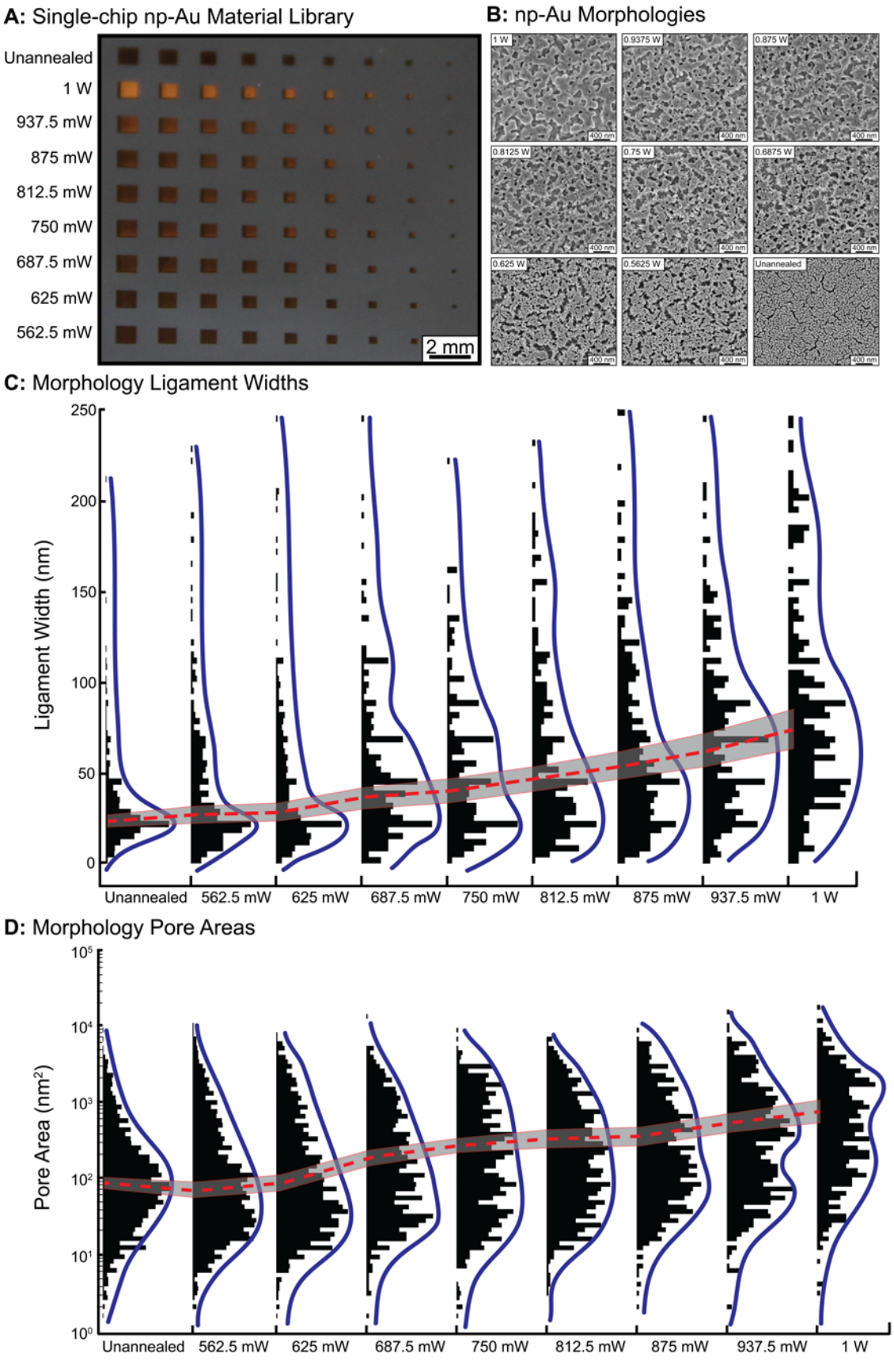
A: Single-chip np-Au Material Library
Unannealed
1 W
937.5 mW
875 mW
812.5 mW
750 mW
687.5 mW
625 mW
562.5 mW
2 mm
B: np-Au Morphologies
1 W
0.9375 W
0.875 W
0.8125 W
0.75 W
0.6875 W
0.625 W
0.5625 W
Unannealed
400 nm
C: Morphology Ligament Widths
Ligament Width (nm)
250
200
150
100
50
0
Unannealed
562.5 mW
625 mW
687.5 mW
750 mW
812.5 mW
875 mW
937.5 mW
1 W
D: Morphology Pore Areas
Pore Area (nm²)
10⁵
10⁴
10³
10²
10¹
10⁰
Unannealed
562.5 mW
625 mW
687.5 mW
750 mW
812.5 mW
875 mW
937.5 mW
1 W

Figure 7. (A) 9 x 9 array of np-Au patterns on single 20 mm silicon chip. Each column contains 9 identical squares spaces 1 mm apart (center to center) with each row decreasing height and width by 100 μm starting at 1 mm height and width (far left) and decreasing to 200 μm height and width (far right). (B) Top down SEM images of each photothermally annealed np-Au morphology on the np-Au material library. (C) Ligament width analysis demonstrates a roughly linear increase in ligament width as laser power is increase past the activation energy. (D) Pore area analysis demonstrates a clear increase in pore size with increasing laser powers, with distributions becoming less dominantly distributed towards smaller pore areas.

The morphologies created on the material library show a roughly linear dependence between ligament widths and pore area versus laser power (Figure 7 C & D). This is an expected result due to the generally linear dependence between the film temperature and applied laser power for the photothermal annealing process. Interestingly, the distributions of ligament width and pore area are altered differently through the process of annealing. The ligament size distribution, originally skewed toward small ligaments, spreads upwards throughout the process of annealing. This is indicative of ligaments joining and creating fewer larger ligaments (Figure 7 C). On the other hand, the entire pore area distribution is shifted towards a larger pore area while the distribution shrinks inward towards the dominant pore size (Figure 7 D). This is most likely due to the thin film having a single average pore size that is the most energetically favorable given the film thickness once enough energy is imparted into the surface diffusion mediated reformation of the np-Au morphology. Here we have shown that single-chip material libraries consisting of a wide and tunable range of morphologies can be easily created through a fast autonomous laser-based micromachining process.

Conclusion

In conclusion, here we have laid out the framework for successful understanding and simulation of the photothermal annealing process for thin film porous materials through investigating laser material coupling, heat distribution in the film, and the mechanism for coarsening in the film. Through this analysis we have demonstrated that continuous-wave irradiation is a superior method for driving surface atom diffusion dominated coarsening while pulsed mode irradiation drives bulk viscous flow of the material. Additionally, we have demonstrated that supporting substrate thermal conductivity plays a crucial role in determining the controllability of the obtainable np-Au morphologies. This has important implications if the fabrication of electrically addressable np-Au material libraries is to be accomplished. Finally, we have shown that for np-Au precision photothermal annealing through the application of a CW (λ = 532 nm) laser effectively controls ligament width and pore diameter changes of np-Au coatings on silicon substrates. This method has been used to create np-Au material libraries consisting of several different morphologies on a single chip. These libraries have the potential to drastically increase the throughput of morphology interaction studies for np-Au specifically in applications such as surface enhanced Raman spectroscopy (SERS),[30] high capacity lithium ion batteries,[31] cell-material interaction studies for neural interfaces,[11, 32] analytical biosensors,[33] as well as nanoscale material science studies.[34] Further optimization of both the material selection (i.e. selecting insulting layers with higher thermal conductivity) and laser parameters (i.e. stable low operating power) is currently underway in order to produce multiple electrode array material libraries. Ultimately this work sets the foundation for understanding laser-based annealing of porous thin film materials and with the fabrication of single chip material libraries has the potential to

increase the throughput of material interaction testing in many disciplines through easy single chip material screening libraries.

Methods

Sample fabrication and characterization: 5 mm-diameter spots of thin films of gold-silver alloy were deposited onto the middle of a piranha cleaned 12 mm-diameter thin (0.15 mm thick) glass slide or onto a bare or lithographically patterned silicon wafer. Gold-silver alloy films (precursor to np-Au) were deposited by direct current sputtering (Kurt. J. Lesker) of a 600 nm-thick gold and silver alloy film (64% silver and 36% gold; atomic %) on top of 80 nm-thick gold corrosion barrier / 50 nm-thick chromium adhesion layer structure,. The np-Au films were obtained by immersing the gold-silver alloy in heated (55°C) nitric acid (70%) for 15 minutes. The short dealloying times used in the present study typically result in residual silver levels in the order of 3-5%.[7, 12]. The samples were then soaked in deionized (DI) water for 24 hours before being dried under nitrogen. **Caution:** Nitric acid is highly corrosive and reactive with organic materials and must be handled with extreme care. The morphology of the coatings was characterized by scanning electron microscopy (FEI Nova NanoSEM430), and elemental compositions before and after dealloying were assessed with energy dispersive X-ray spectroscopy (Oxford INCA, Energy-EDS). Average ligament width was analyzed using a custom MATLAB script by averaging both vertically and horizontally over each SEM image taken. Pore area was calculated through a custom contour finding program written in Python.

Photothermal annealing of np-Au films: Photothermal laser annealing was carried out either with a continuous-wave (CW) laser (experimental set-up shown in Figure 1 of the supporting information) or a pulsed laser mill (New Wave Research, Fremont, CA). In the CW mode set-up, a CW laser (SproutD, Lighthouse Photonics) operating at a wavelength of λ = 532 nm was focused in 5 μm spot onto the sample through a 5X objective (Mitutoyo M Plan Apo 5x). Samples were mounted on a motorized XY stage (ASI MS2000) with manual Z axis control for focus. The stage allows for movement in a 100 mm range in both the X and Y directions at a speed up to 7 mm/s (500 μm/s used for this study). Stage, laser, shutter, and camera control was accomplished through a self-written LabVIEW control program that enables the complete automation of the laser processing.

Fabrication of np-Au single chip material libraries: Np-Au material libraries were fabricated on a single chip through traditional microfabrication photolithography, deposition, and liftoff stages all done using the Center for Nano and Micro-manufacturing clean room at the University of California, Davis. In short, silicon wafers (University Wafer) were spun with ~2 μm of AZ 5214E-IR (Clariant) and patterned using a film mask. Alloy deposition was carried out as per the previously mentioned protocol. After deposition photoresist was lifted through exposure to N-Methyl-2-pyrrolidone (NMP) for ~4 hours.

Supporting Information

Details of sample preparation, fabrication of material libraries, as well as further analysis and supporting scanning electron micrographs can be found in Supporting Information. This material is available free of charge via the Internet at http://pubs.acs.org

Corresponding Author

Author Contributions
The manuscript was written through contributions of all authors. All authors have given approval to the final version of the manuscript.

Acknowledgements
We gratefully acknowledge the support from UC Lab Fees Research Program Award [12-LR-237197], Research Investments in the Sciences & Engineering (RISE) Award, and UC Davis College of Engineering start-up funds. C. Chapman was supported by a National Science Foundation Graduate Research Fellowship [DGE-1148897] and a predoctoral fellowship from the National Institute of Health [T32-GM008799]. Any opinion, findings, and conclusions or recommendations expressed in the material are those of the authors(s) and do not necessarily reflect the views of the National Science Foundation or the National Institutes of Health. Work at LLNL was performed under the auspices of the U.S. DOE by LLNL under Contract DE-AC52-07NA27344.

References:
1. Seker, E., Reed, M. L. & Begley, M. R., Nanoporous Gold: Fabrication, Characterization, and Applications. *Materials* **2009,** *2*, 2188-2215.
2. Santos, G. M., Zhao, F., Zeng, J. & Shih, W., Characterization of Nanoporous Gold Disks for Photothermal Light Harvesting and Light-Gated Molecular Release. *Nanoscale* **2014,** *6*, 5718-5724.
3. Li, K., Huang, J., Shi, G., Zhang, W. & Jin, L., A Sensitive Nanoporous Gold-Based Electrochemical DNA Biosensor for *Escherichia Coli* Detection. *Anal. Lett.* **2011,** *44*, 2559-2570.
4. Feng, J., Zhao, W. & Wu, J., A Label-Free Optical Sensor Based on Nanoporous Gold Arrays for the Detection of Oligodeoxynucleotides. *Biosens. Bioelectron.* **2011,** *30*, 21-27.
5. Jin, H. J. W., J., A Material with Electrically Tunable Strength and Flow Stress. *Science* **2011,** *332*, 1179-1182.
6. Fujita, T., Guan, P., McKenna, K., Lang, X., Hirata, A., Zhang, L., Tokunaga, T., Arai, S., Yamamoto, Y., Tanaka, N., Ishikawa, Y., Asao, N., Yamamoto, Y., Erlebacher, J. & Chen, M., Atomic Origins of the High Catalytic Activity of Nanoporous Gold. *Nat. Mater.* **2012,** *11*, 775-780.
7. Kurtulus, O., Daggumati, P. & Seker, E., Molecular Release from Patterned Nanoporous Gold Thin Films. *Nanoscale* **2014,** *6*, 7062-7071.
8. Gittard, S., Pierson, B., Ha, C., Wu, C., Narayan, R. & Robinson D., Supercapacitive Transport of Pharmacologic Agents Using Nanoporous Gold Electrodes. *Biotechnol. J.* **2010,** *5*, 192-200.
9. Hodge, A. M., Hayes, J. R., Caro, J. A., Biener, J. & Hamza, A. V., Characterization and Mechanical Behavior of Nanoporous Gold. *Adv. Eng. Mater.* **2006,** *8*, 853-857.
10. Lee, D., Wei, X., Chen, X., Zhao, M., Jun, S. C., Hone, J., Herbert, E. G., Oliver, W. C. & Kysar, J. W., Microfabrication and Mechanical Properties of Nanoporous Gold at the Nanoscale. *Scr. Mater.* **2007,** *56*, 437-440.
11. Chapman, C. A. R., Chen, H., Stamou, M., Biener, J., Biener, M. M., Lein, P. J. & Seker, E., Nanoporous Gold as a Neural Interface Coating: Effects of Topography, Surface Chemistry, and Feature Size. *ACS Appl. Mater. Interfaces* **2015**.

12. Seker, E., Berdichevsky, Y., Begley, M.R., Reed, M.L., Staley, K.J. & Yarmush, M.L., The Fabrication of Low-Impedance Nanoporous Gold Multiple-Electrode Arrays for Neural Electrophysiology Studies. *Nanotechnology* **2010,** *21*, 1-7.
13. Seker, E., Berdichevsky, Y., Staley, K.J. & Yarmush, M.L., Microfabrication-Compatible Nanoporous Gold Foams as Biomaterials for Drug Delivery. *Adv. Healthcare Mater.* **2012,** *1*, 172-176.
14. Erlebacher, J., Aziz, M. J., Karma, A., Dimitrov, N. & Sieradzki, K., Evolution of Nanoporosity in Dealloying. *Nature* **2001,** *410*, 450-453.
15. Hakamada, M. M., M., Thermal Coarsening of Nanoporous Gold: Melting or Recrystallization. *J. Mater. Res.* **2008,** *24*, 301-304.
16. Forty, A. J. D., P., A Micromorphological Study of the Dissolution of Silver-Gold Alloys in Nitric Acid. *Philos. Mag. A* **1980,** *42*, 295-318.
17. Qian, L. H. C., M. W., Ultrafine Nanoporous Gold by Low-Temperature Dealloying and Kinetics of Nanopore Formation. *Appl. Phys. Lett.* **2007,** *91*, 083105-1-083105-3.
18. Li, R. S., K., Ductile-Brittle Transition in Random Porous Au. *Phys. Rev. Lett.* **1992,** *68*, 1168-1171.
19. Hakamada, M. M., M., Microstructural Evolution in Nanoporous Gold by Thermal and Acid Treatments. *Mater. Lett.* **2008,** *62*, 483-486.
20. Schade, L., Franzka, S., Mathieu, M., Biener, M. M., Biener, J & Hartmann, N., Photothermal Laser Microsintering of Nanoporous Gold. *Langmuir* **2014,** *30*, 7190-7197.
21. Dorofeeva, T. S. S., E., Electrically-Tunable Pore Morphology in Nanoporous Gold Thin Films. *Nano Res.* **2015**.
22. Elhadj, S., Matthews, M. J. & Yang S. T., Combined Infrared Thermal Imaging and Laser Heating for the Study of Materials Thermophysical and Processing Properties at High Temperatures. *Critical Reviews in Solid State and Materials Sciences* **2014,** *39*, 175-196.
23. Guss, G. M., Sridharan, A. K., Elhadj, S., Johnson, M. A. & Matthews M. J., Nanoscale Surface Tracking of Laser Material Processing Using Phase Shifting Diffraction Interferometry. *Optics Express* **2014,** *22*, 14493-14504.
24. Matthews, M. J., Yang, S. T., Shen, N., Elhadj, S., Raman, R. N., Guss, G., Bass, I. L., Nostrand, M. C. & Wegner, P. J., Micro-Shaping, Polishing, and Damage Repair of Fused Silica Surface Using Focused Infrared Laser Beams. *Adv. Eng. Mater.* **2014,** *17*, 247-252.
25. Schade, L., Franzka, S., Hardt, S., Wiggers, H. & Hartmann, N., Sintering of Thin Titanium Dioxide Nanoparticle Films Via Photothermal Processing with Ultraviolet Continuous-Wave Lasers. *Appl. Surf. Sci.* **2013,** *278*, 336-340.
26. Wang, J., Xia, R., Zhu, J., Ding, Y., Zhang, X. & Chen Y., Effect of Thermal Coarsening on the Thermal Conductivity of Nanoporous Gold. *J. Mater. Sci.* **2011,** *47*, 5013-5018.
27. Hopkins, P. E., Norris, P. M., Phinney, L. M., Policastro, S. A. & Kelly, R. G., Thermal Conductivity in Nanoporous Gold Films During Electron-Phonon Nonequilibrium. *J. Nanomater.* **2008,** *2008*, 7.
28. Gobel, H. v. B., P., A Study of Surface Diffusion on Gold with an Atomic Force Microscope. *Surf. Sci.* **1995,** *331*, 885-890.
29. Cassidy, D. C. G., N. A., Capillarity-Induced Smoothing of Glass Surfaces by Viscous Flow. *J. Am. Ceram. Soc.* **1969,** *53*, 161-168.
30. Bianco, G. V., Giangregorio, M. M., Losurdo, M., Capezzuto, P. & Bruno, G., Supported Faceted Gold Nanoparticles with Tunable Surface Plasmon Resonance for Nir-Sers. *Adv. Func. Mater.* **2012,** *22*, 5081-5088.

31. Ye, J., Baumgaertel, A. C., Wang, Y. M., Biener, J. & Biener, M. M., Structural Optimization of 3d Porous Electrodes for High-Rate Performance Lithion Ion Batteries. *ACS Nano* **2015,** *9,* 2194-2202.
32. Tan, Y. H., Terrill, S.E., Paranjape, G.S., Stine, K.J. & Nichols M.R., The Influence of Gold Surface Texture on Microglia Morphology and Activation. *Biomater. Sci.* **2014,** *2,* 110-120.
33. Daggumati, P., Matharu, Z. & Seker, E., Effect of Nanoporous Gold Thin Film Morphology on Electrchemical DNA Sensing. *Anal. Chem.* **2015**.
34. Biener, M. M., Biener, J., Wang, Y. M., Shin, S. J., Tran, I. C., Willey, T. M., Perez, F. N., Poco, J. F., Gammon, S. A., Fournier, K. B., van Buuren, A. W., Statcher, J. H. & Hamza, A. V., Atomic Layer Deposition-Derived Ultra-Low-Density Composite Bulk Materials with Deterministic Density and Composition. *ACS Appl. Mater. Interfaces* **2013,** *5,* 13129-13134.